e-Polymers **2009**, no. 053

http://www.e-polymers.org

ISSN 1618-7229

Vitrification and devitrification of the rigid amorphous fraction in poly(ethylene terephthalate)

Maria Cristina Righetti,[1] * *Maria Laura Di Lorenzo*[2]

[1*]Istituto per i Processi Chimico-Fisici (CNR) – Area della Ricerca CNR – Via G. Moruzzi, 1 – 56124 Pisa – Italy; fax: +39-050-3152230; e-mail righetti@ipcf.cnr.it
[2]Istituto di Chimica e Tecnologia dei Polimeri (CNR) – c/o Comprensorio Olivetti – Via Campi Flegrei, 34 – 80078 Pozzuoli (NA) – Italy; fax: +39-081-8675230; e-mail marialaura.dilorenzo@ictp.cnr.it

(Received: 22 December, 2007; published: 31 May, 2009)

Abstract: Vitrification and devitrification of the rigid amorphous fraction (RAF) of poly(ethylene terephthalate) (PET), analyzed during development and disappearance of the three phase structure, are detailed in this contribution. Upon cooling from the melt at a constant rate, the rigid amorphous fraction starts to vitrify when the crystallization process is almost finished, and continues on further cooling. The rigid amorphous fraction is formed in the same temperature range of the secondary crystal growth. Analysis of the low melting endotherm that is observed in isothermally crystallized PET a few degrees above the crystallization temperature reveals a joint contribution of melting and devitrification of the rigid amorphous fraction. The results confirm a link between secondary crystallization and vitrification of the rigid amorphous fraction in semicrystalline polymers. Secondary crystallization takes place in geometrically restricted areas, in which the polymer chains undergo large constraints, so that the mobility of the amorphous chain portions coupled with the crystal phase is reduced. Similarly, the gain in mobility upon partial melting of thinner and/or more defective crystals allows an increase in mobility of the coupled amorphous regions, which results in concurrent mobilization of the rigid amorphous fraction.

Introduction

The concept of three-phase structure for semicrystalline polymers was first hypothesized in mid ‘80s, upon observation of a deficiency in heat capacity jump at the glass transition [1-2]: in addition to the crystalline fraction (CF) and the mobile amorphous phase (MAF), a third fraction of nanosized dimensions was introduced. The latter, named “rigid amorphous fraction” (RAF), is made of the amorphous chain portions that are closely connected to the ordered crystalline phase. The crystal phase exerts constraints on the nearby amorphous chain portions constituting the rigid amorphous fraction, which has a reduced mobility compared to the mobile amorphous phase [3].

The existence of the RAF has been probed by a number of experimental techniques, including ^{13}C solid state NMR [4-8], X-ray diffraction [7], and electron microscopy [5]. Despite the high scientific interest that has led to a large amount of studies, recently reviewed in Ref. [3], properties of the rigid amorphous fraction are still largely unknown.

The experimental technique most widely used to quantify the rigid amorphous content in semicrystalline polymers is calorimetry, both in the conventional and

temperature-modulated modes [3]. The glass transition (T_g) of the RAF is often located between the T_g of the unstrained amorphous phase and the melting temperature, but this is not a general rule. Some semicrystalline polymers may have no RAF, or may have a RAF with a glass transition that coincides with melting, or even above the melting point [3]. For poly(oxy-2,6-dimethyl-1,4-phenylene) it was shown that the RAF glass transition temperature, higher than the melting point, delays fusion and shifts it to a higher temperature until enough mobility is present at the crystal surface [9]. Similarly, a possible influence of the rigid amorphous fraction on multiple melting behavior and reversibility of the melting process was hypothesized for poly(butylene terephthalate) [10].

The kinetics of formation of the RAF in relation with the other phases has been investigated for a limited number of polymers [11-15]. Upon isothermal crystallization, conducted at a single temperature, parallel development of RAF and crystallinity was probed for poly(3-hydroxybutyrate) and polycarbonate, whereas only partial formation of the RAF during crystallization was evidenced for syndiotactic polypropylene [11-13]. In these studies the concurrent development of both the crystal phase and the rigid amorphous fraction was followed at a single temperature. A new method that allows to monitor simultaneously the development of crystalline, mobile amorphous and rigid amorphous fractions during cooling from the melt, was recently presented [16-17]. On the basis of the results obtained by means of this new method, details about the devitrification of the RAF in PET, gained on heating by temperature-modulated calorimetry (TMDSC), are discussed here.

Glassy materials have a thermodynamic non-equilibrium nature; as a result, the physical and mechanical properties of these materials evolve toward the equilibrium state. Thus some enthalpy recovery, revealed by calorimetric analysis as an endothermic peak, is generally associated on heating to the glass transition of the MAF. Similarly also for the RAF, which is an amorphous, and therefore metastable state, one would expect a decrease of enthalpy with time, which, during a successive heating, should yield an endotherm.

An endothermic peak (sometimes called ‘annealing peak’) is often observed upon heating an isothermally crystallized polymer, at about 10-30 °C above the crystallization temperature. Such behavior has been observed for a number of polymers, including PET [18], poly(phenylene sulfide) (PPS) [19], and isotactic polystyrene [20], but its nature, whether the endotherm is associated to partial melting or to enthalpy recovery of the rigid amorphous fraction is still under debate. Recently it has been demonstrated that for PET the origin of this endotherm is connected with both partial fusion of the crystalline portions and enthalpy recovery subsequent to structural relaxation of the rigid amorphous fraction [21]. The result was achieved through a new method of analysis of the modulated heat flow rate curves from temperature-modulated differential scanning calorimetry (TMDSC). In the present paper further considerations on the thermal events occurring in correspondence with the ‘annealing peak’ are presented and discussed.

Results and discussion

The conventional and temperature-modulated calorimetry analyses of PET upon cooling from the melt at -2 °C/min are presented in Figure 1 together with thermodynamic heat capacity data as taken from the ATHAS Data Bank [22]. The conventional DSC plot ($c_{p,tot}$) reveals a large exotherm starting from 227 °C, with a

peak centered at 215.5 °C and a long tail that gradually approaches the baseline heat capacity (c_p). At lower temperatures the $c_{p,tot}$ evidences the occurrence of the glass transition of the MAF ('bulk' glass transition), that ranges from about 100 to 65 °C and is centered at 85 °C. The mobile amorphous fraction at 100 °C, calculated as the ratio between the experimental c_p step and the c_p step of fully amorphous PET, which is obtained from the ATHAS Data Bank [22], is equal to 0.37.

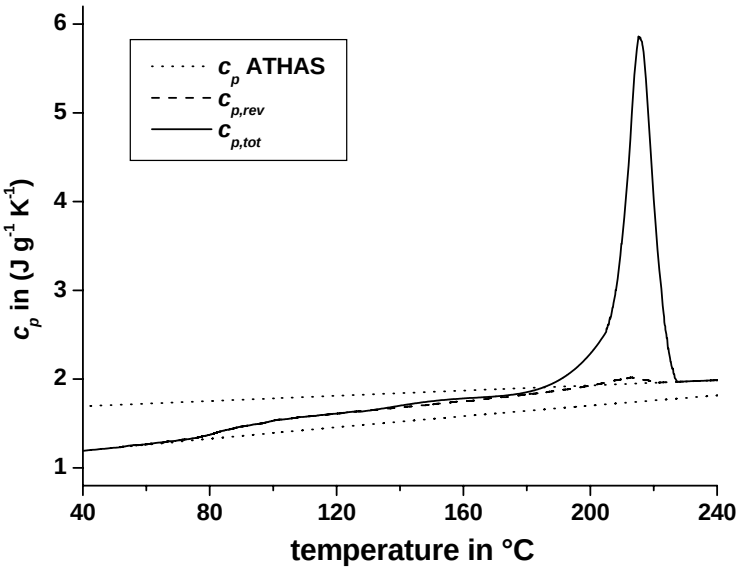

Fig. 1. Total specific heat capacity ($c_{p,tot}$) and reversing specific heat capacity ($c_{p,rev}$) of PET in the crystallization region on cooling at -2 °C min^{-1} as a function of temperature. The dotted lines are the crystalline and amorphous specific heat capacities as available from the ATHAS data bank [22].

The reversing specific heat capacity ($c_{p,rev}$) curve, determined with temperature-modulated calorimetry, displays a small peak centered at 213 °C, which is much less intense than the exotherm measured with standard DSC. Below 170 °C the $c_{p,rev}$ trend becomes linear down to the glass temperature. The small peak centered at 213 °C in the $c_{p,rev}$ curve arises from loss of stationary conditions, changes in crystallization rate occurring in the two semiperiods and, perhaps a reversing crystallization/melting process [16, 23]. The first effect originates from the intense and fast crystallization process, that causes lack of accuracy in the calculation of reversing heat capacity with the procedure summarized in the Experimental part, due to erroneous description of the modulated signal with a Fourier series [24], the second and third effects reveal possible latent heat contributions to the $c_{p,rev}$ curve beyond the thermodynamic c_p. Only below 170 °C, on completion of this small apparent endotherm, the reversing specific heat capacity corresponds to the baseline specific heat capacity, i.e. the specific heat capacity without contributions from latent heat effects, as previously proven by the analysis of the modulated heat flow rate profile, which shows in the temperature range 170-100 °C no deviation from the ideal rectangular-shaped wave [16]. Therefore under the chosen experimental conditions, a quantitative separation of reversible and irreversible events is possible only at temperatures lower than 170 °C [16].

The experimental data presented in Figure 1 were used to determine the kinetics of evolution of the crystalline, mobile amorphous and rigid amorphous fractions of PET during cooling. The enthalpy of a material can be expressed as the sum of the thermodynamic enthalpy of the various phases, weighted by the phase content. In case only one amorphous phase and one crystalline phase are taken into account (two-phase model), the experimental enthalpy is:

$$h(T) = m_C(T)h_C(T) + m_A(T)h_A(T) \quad (1)$$

where $m_C(T)$ and $m_A(T)$ are the crystal and mobile amorphous mass fractions, with $[m_C(T)+m_A(T)] = 1$, and $h_C(T)$ and $h_A(T)$ the temperature-dependent enthalpies of the crystalline and mobile amorphous polymer respectively. From eq. (1), the crystal content can be determined as:

$$m_C(T) = \frac{h_A(T) - h(T)}{h_A(T) - h_C(T)} \quad (2)$$

being $[h_A(T)-h(T)]$ easily obtained through integration of the experimental heat capacity data [25-26] and the difference $[h_A(T)-h_C(T)]$ available from the ATHAS Data Bank for more than 200 different polymers [22]. Similarly, the enthalpy of a three-phase system comprising also a rigid amorphous fraction can be expressed in terms of the enthalpy of the three fractions:

$$h(T) = m_C(T)h_C(T) + m_A(T)h_A(T) + m_{RA}(T)h_{RA}(T) \quad (3)$$

where $m_{RA}(T)$ is the mass fraction of the RAF and $h_{RA}(T)$ the corresponding enthalpy. Being $m_C(T)+m_A(T)+m_{RA}(T)=1$, eq (3) can be rewritten as:

$$m_C(T) = \frac{h_A(T) - h(T)}{h_A(T) - h_C(T)} + m_{RA}(T)\frac{h_{RA}(T) - h_A(T)}{h_A(T) - h_C(T)} \quad (4)$$

from which it results that the crystalline mass fraction for a three-phase model is given by the value calculated for the two-phase model [see eq (2)], plus a term related to both the content and the specific enthalpy of the rigid amorphous fraction. From eq. (4), as detailed in Ref. 16 and 26, the temperature dependence of the experimental heat capacity in a three-phase system is obtained:

$$c_p(T) = m_C(T)c_{p,C}(T) + m_A(T)c_{p,A}(T) + m_{RA}(T)c_{p,C}(T) - [h_A(T) - h_C(T)]\frac{dm_C(T)}{dT} \quad (5)$$

An expression describing the crystalline mass fraction m_C as a function of temperature during cooling from the melt was derived from eq. (4) [16]:

$$m_C(T) = \frac{h_A(T) - h(T)}{h_A(T) - h_C(T)} + \frac{\int_{T_1}^{T}[m_S(T') - m_C(T')][c_{p,C}(T') - c_{p,A}(T')]dT'}{h_A(T) - h_C(T)} \quad (6)$$

where T_1 is a reference temperature in the melt at which no RAF and crystals are present, so that $h(T_1)=h_A(T_1)$, and m_S is the solid mass fraction, defined as follows:

$$m_S(T) = m_C(T) + m_{RA}(T) = 1 - m_A(T) \quad (7)$$

For a three-phase system the crystalline mass fraction $m_C(T)$ can be attained from eq. (6) with a successive approximations method by using as initial $m_C(T)$ function the crystalline mass fraction from the two-phase method [eq. (2)] and after determination of the total solid content $m_S(T)$. The latter can be gained from eq. (7)

through the baseline specific heat capacity, $c_{p,base}$, i.e. the specific heat capacity without contributions from latent heat, being:

$$m_A(T) = \frac{c_{p,base}(T) - c_{p,C}(T)}{c_{p,A}(T) - c_{p,C}(T)} \quad (8)$$

As detailed above, loss of stationary conditions in the TMDSC analysis, as well as possible latent heat effects, both occurring in the temperature range of the small apparent endotherm in the $c_{p,rev}$ curve, allow to obtain the baseline c_p only at temperatures lower than 170 °C. As a first approximation, the baseline c_p was extrapolated linearly up to the melt. The $m_S(T)$ curve calculated from the linear baseline c_p is presented in Figure 2 together with the $m_C(T)$ curves calculated according to the two-phase model [eq. (2)]. Intersection of the $m_S(T)$ curve with the $m_C(T)$ plot occurs at 175 °C. It can be safely hypothesized that the two phase and three-phase models can be applied to describe the thermal behavior of PET cooled at a rate of -2 °C/min at temperatures respectively higher and lower than 175 °C, i.e. above and below the intersection point of Figure 2.

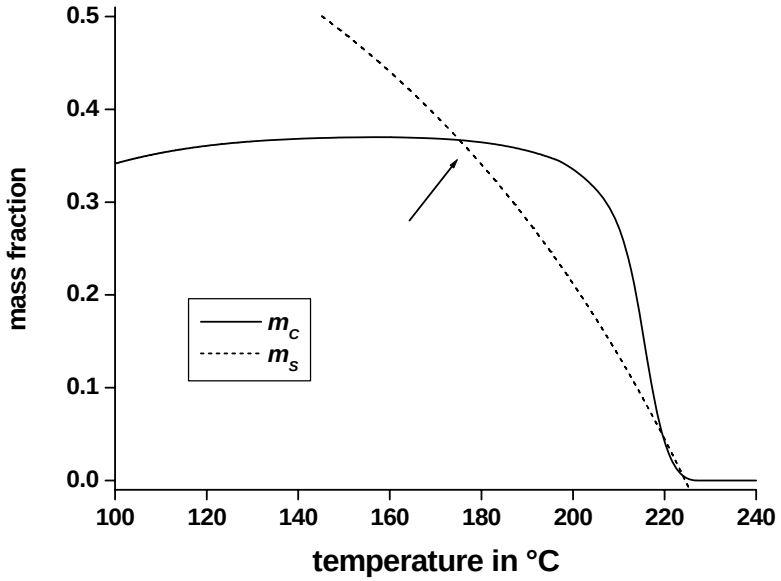

Fig. 2. Crystalline mass fraction (m_C) from the enthalpy-based two-phase method (solid line) and solid mass fraction (m_S) calculated with eq (7) and (8) on cooling at -2 °C as a function of temperature.

Since the mobile amorphous fraction $m_A(T)$, and therefore $m_S(T)$, can be calculated in the temperature range from 100 to 175 °C, i.e. up to the intersection point of Figure 2, with a small approximation only in proximity of the superior limit of this interval, the crystalline mass fraction $m_C(T)$ for a three-phase system was determined using eq. (6). At temperatures higher than the intersection points, where $m_S(T) = m_C(T)$, being $m_{RA}(T) = 0$, the integral in eq. (6) is zero and the crystalline mass fraction is described by the relationship for the two-phase model. After determination of $m_C(T)$ in the temperature region in which the three-phase model holds, the RAF content is obtained by difference from $m_S(T)$.

The temperature dependences of m_C, m_A and m_{RA} in the whole crystallization range are presented in Figure 3. The cusps in the $m_A(T)$ and $m_{RA}(T)$ curves arise from the sharp mathematical switch from one model to the other, as well as from the incomplete accuracy of the linear extrapolation of $c_{p,base}(T)$ from 170 °C up to the intersection point of Figure 2. From the data shown in Figure 3 it can be drawn that non-isothermal crystallization of PET from the melt at -2 °C/min leads to a crystal fraction of 0.38 at 100 °C, a rigid amorphous content of 0.25, and a mobile amorphous phase amounting to 0.37. Most important is that the kinetics of vitrification of the RAF in PET is only partially linked to the crystallization process, as the rigid amorphous structure starts to vitrify during the final stages of non-isothermal crystallization, with full establishment of the rigid amorphous structure completed during the subsequent cooling to room temperature. The simultaneous development of the rigid amorphous structure and of the final portions of the crystal phase may have implications on the kinetics of devitrification of the RAF, as discussed below.

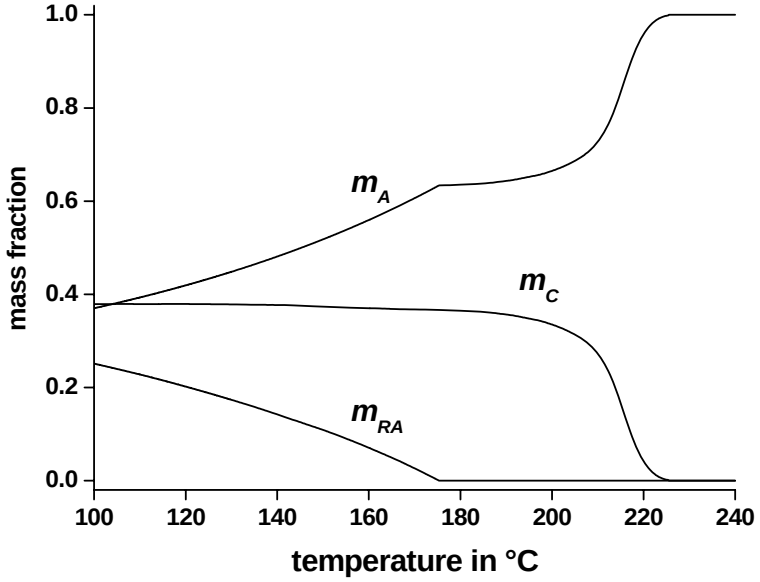

Fig. 3. Crystalline mass fraction (m_C), mobile amorphous mass fraction (m_A) and rigid amorphous mass fraction (m_{RA}) as a function of temperature. The curves in the temperature range between 100 °C and the intersection point of Figure 2 are from the enthalpy-based three-phase method, those in the temperature range between the intersection points and 240 [°C from the enthalpy-based two-phase method.

The procedure used to determine the evolution of the three nanophases of PET during cooling from the melt cannot be applied to monitor the mobilization of the rigid fractions upon heating at a constant rate, due to the difficulties in obtaining the baseline heat capacity curve in a wide temperature range from TMDSC analysis [27]. The latter is caused by the large reorganization of the crystal phase during melting, that results in an increase of the $c_{p,rev}$ curve [28], and by a high probability of occurrence of reversing melting/crystallization events upon heating.

In order to derive information on devitrification of the rigid amorphous fraction in PET, the thermal behavior after isothermal crystallization was investigated. As mentioned in the Introduction Section, DSC plots of isothermally crystallized poly(ethylene

terephthalate), similarly to other semicrystalline polymers, display a small endotherm (annealing peak) a few degrees above the crystallization temperature. Examples are shown in Figure 4, which presents the specific heat capacity curves of poly(ethylene terephthalate) determined upon heating after isothermal crystallization at the indicated T_c's for 1 h and subsequent quenching to room temperature. Both the curves show, besides the main melting peak located around 230-260 °C, a small endotherm at circa 10 °C above the isothermal crystallization temperature. The origin of the so-called annealing peak has been ascribed either to partial melting or to enthalpy recovery of the rigid amorphous fraction [18-20]. Recently it was demonstrated that for PET this endotherm is connected with both partial fusion of the crystalline portions and enthalpy recovery subsequent to structural relaxation of the RAF [21]. The investigation method was based on a new interpretation of the modulated heat flow rate curves from TMDSC runs. The procedure consists in the analysis of the steady-state heat flow rate signal in the heating and cooling semiperiods, with the temperature modulation performed by a sawtooth profile [21]. The study was conducted in parallel on the evolution of the total specific heat capacity and of the reversing specific heat capacity of PET samples crystallized for 1 h at various T_c. In order to shed further light on the thermal events occurring in correspondence with the annealing peak, and on the possible relation between formation and disappearance of the solid fractions in PET, TMDSC experiments on samples isothermally crystallized for different times are here presented and discussed.

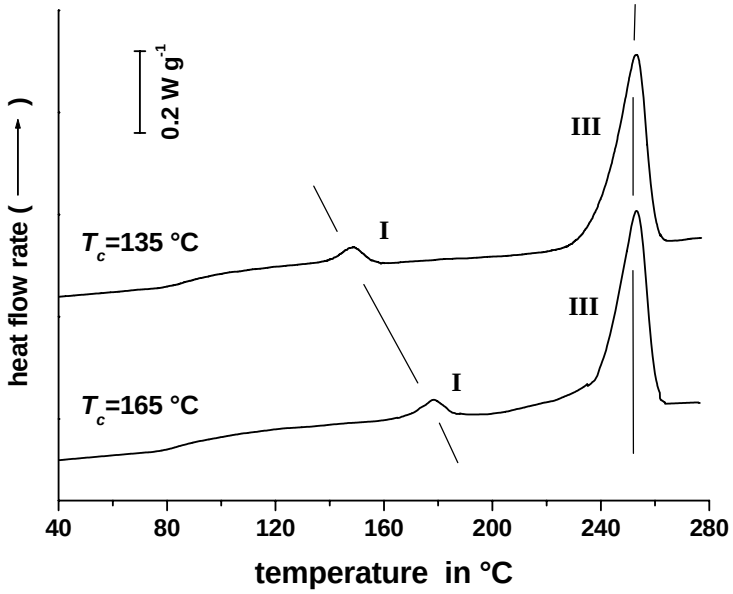

Fig. 4. Heat flow rate curves of PET as a function of temperature, after isothermal crystallization (1 h) at the indicated T_c (heating rate: 10 °C min^{-1}). The thin lines are guides for the eye.

Figure 5 illustrates the total and reversing specific heat capacity curves of PET after crystallization at 135 °C for 1 h and 16 h and successive rapid cooling to room temperature. Slight changes in the m_C, m_A and m_{RA} contents with the duration of the isotherm can be deduced from these data, as quantified below. The annealing peak,

shown by the $c_{p,tot}$ curves and centered at 144 °C after isothermal crystallization for 1 h, shifts to higher temperatures and increases in intensity after crystallization for 16 h. Other experiments, reported in Ref. [21], demonstrated that the intensity of the annealing peak decreased with reducing the length of the isotherm at 135 °C up to the obtainment of complete crystallization (22 min).

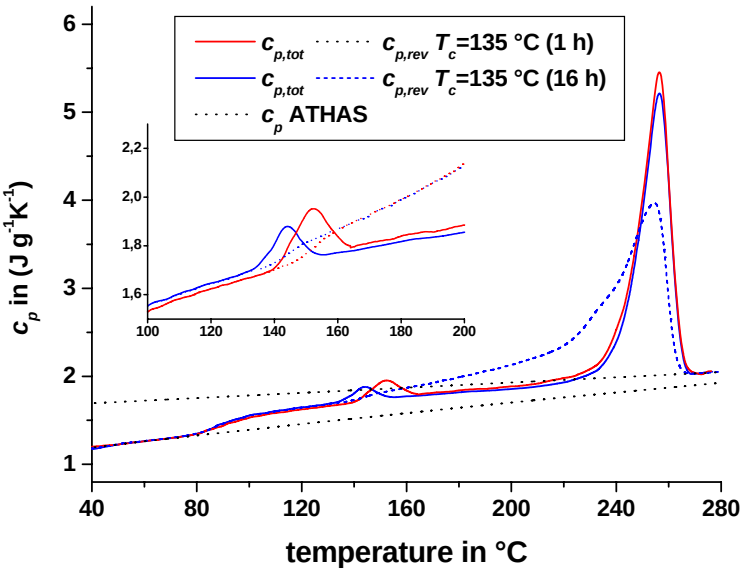

Fig. 5. Total specific heat capacity ($c_{p,tot}$: solid line) and reversing specific heat capacity ($c_{p,rev}$: dash line) of PET as a function of the underlying temperature, after crystallization for 1 h and 16 h at 135 °C (blue and red lines respectively). (The underlying temperature is obtained by averaging the temperature over the modulation period.) The crystalline and mobile amorphous specific heat capacities, as taken from ATHAS Data Bank [22], are also shown as dot lines. In the insert an enlargement of the Figure is reported.

As better evidenced in the insert of Figure 5, in correspondence with the annealing peak the $c_{p,rev}$ curves display a step, which appears more intense after the longer crystallization time. This behavior, characterized by a jump in the $c_{p,rev}$ plot and a peak in the $c_{p,tot}$ curve, is typical of a glass transition coupled with enthalpy recovery [29]. However, in case only devitrification and enthalpy recovery occur, one would expect that the $c_{p,tot}$ and $c_{p,rev}$ curves coincide after completion of the thermal event, which is not observed in Figure 5, as at the end of the transition the $c_{p,rev}$ curves are higher than the respective $c_{p,tot}$ plots. Moreover, the $c_{p,rev}$ step exceeds the value of the amorphous specific heat capacity, as shown in Figure 5. All these findings exclude the possibility that the thermal event under investigation originates only from the glass transition of the RAF overlapped with enthalpy recovery. The fact that at temperatures higher than the annealing peak the values of $c_{p,rev}$ are higher than $c_{p,tot}$ suggests that additional thermal events, involving both endothermic and exothermic latent heats, occur during the temperature modulation. In fact, for a power-compensation calorimeter, the temperature amplitude is not affected by thermal events, whereas the amplitude of the heat flow rate (A_{HF}) originates from the sum of the absolute values of the reversing endothermic and exothermic events intensity, which results in an increase of $c_{p,rev}$ (see Experimental part). Conversely, in the total

specific heat capacity the latent heats released or absorbed sum algebraically, so that the $c_{p,tot}$ values appear lower than $c_{p,rev}$ [28]. It is worth noting the $c_{p,rev}$ curves gained after isothermal crystallization at 135 °C for 1 and 16 h perfectly overlap at temperatures higher than the annealing peak, which proves that the 'reversing' melting/crystallization above the annealing peak is quite insensible of the different crystallinity level reached after prolonged annealing at 135 °C.

From the insert of Figure 5 it can be evidenced that at temperatures lower than the annealing peak the experimental c_p of the sample crystallized for 16 h is lower than that crystallized for a shorter time, which, as expected, witnesses a higher percentage of solid material. An approximate estimation of the three fractions (crystalline, mobile amorphous and rigid amorphous) present at 135 °C, i.e. before the annealing peak, in the PET samples crystallized for 1 h and 16 h respectively, was performed. The mobile amorphous content was obtained according to Eq. (8), from $c_{p,rev}$ at 135 °C, which can be used as baseline heat capacity values; the values of crystalline fraction m_c was estimated by integration of the endothermic peaks evolved during the TMDSC runs and described by the $c_{p,tot}$ curves; the rigid amorphous content was determined by difference. The results are: m_A=0.57, m_C=0.34 m_{RA}=0.09 for PET crystallized 1 h at 135 °C and m_A=0.51, m_C=0.42 m_{RA}=0.07 for PET crystallized 16 h at 135 °C. Since the m_C values are quite approximate, mostly because the baseline used for the integration does not account for devitrification of the rigid amorphous fraction and because they include also the crystallinity increase occurring during the TMDSC runs, it comes out that the crystal and rigid amorphous contents result over- and underestimated, respectively. Anyway, the lower m_{RA} content determined after 16 h of permanence at 135 °C is in excellent agreement with the findings reported in Ref. [15], according to which crystallinity of PET increases during annealing at the expense of the rigid amorphous fraction.

The presence of RAF at 135 °C attests that the rigid amorphous fraction develops, at least partly, during the isothermal crystallization event [15]. In fact, if further RAF vitrifies during the cooling that follows isothermal crystallization, this fraction should mobilize on heating as a normal glass transition event, that is around the same temperature at which it develops. This suggests that the endothermic peak observed on heating just above T_c may contain also contributions of enthalpy recovery connected to the mobilization of the RAF.

In order to verify if enthalpy recovery of the rigid amorphous fraction overlaps the initial fusion in PET, additional analyses of the TMDSC data were conducted using the method proposed in Ref. [21]. Besides the common mathematical treatment of the modulated signal by approximation with a Fourier series, that was used to obtain the reversing c_p plots illustrated in Figures 1 and 5, some unusual description of the heat flow rate resulting from the temperature modulation program was attempted. As detailed in the Experimental Part, temperature modulation was built with a sawtooth program. The modulated heat flow rate curves were analyzed by treating them as sequences of conventional DSC steps, obtained with alternating heating and cooling segments. Every time the scanning rate is reversed, the TMDSC apparatus undergoes a momentary loss of steady-state, evidenced by a sharp increase or decrease of the heat flow rate, then, when steady-state is reached, the heat flow rate signal contains only contributions deriving from the intrinsic c_p of the sample and from thermal events that may lead to upward or downward deflections of the heat flow rate.

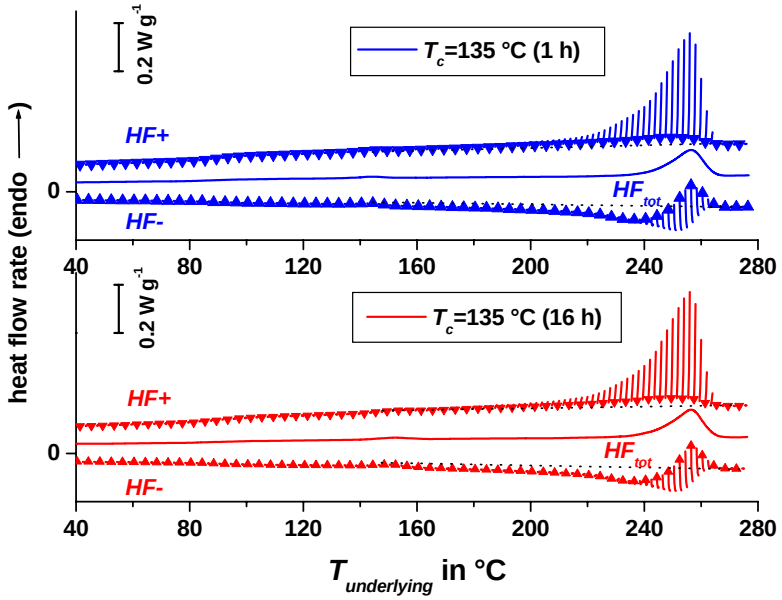

Fig. 6. Steady-state heat flow rate curves of PET in the heating and cooling semiperiods (*HF*+ and *HF*- respectively), after isothermal crystallization for 1 h and 16 h at 135 °C (blue and red lines respectively) as a function of the underlying temperature. The initial points of the steady-state are evidenced by symbols (heating semiperiod: ▼; cooling semiperiod: ▲). The total heat flow rate curve (HF_{tot}) is also drawn. The dashed lines are the baselines in the melting-crystallization/recrystallization region.

Using a home-built software, the initial transients of the two semiperiods were eliminated, which allowed to analyze the steady-state heat flow rate portions of the raw TMDSC. Figure 6 shows the steady-state heat flow rate curves in the heating (*HF*+) and cooling (*HF*-) semiperiods after isothermal crystallization (1 h and 16 h respectively) at 135 °C, together with the corresponding HF_{tot} curves. In Figure 6 the initial points of the steady-state are evidenced by symbols, whereas the dashed lines are approximated baselines in the melting-crystallization/recrystallization regions. Since differences between the two crystallization conditions are not appreciable with the scales used in Figure 6, enlargements in the temperature interval in which the annealing peak takes place are displayed in Figure 7.

Starting from about 135 °C and 140 °C, ascendant deviations in the envelopes of the initial points of *HF*+ and *HF*- are exhibited in Figure 7 by the PET samples crystallized for 1 h and 16 h respectively, from which the occurrence of an endothermic irreversible process, i.e. a process that takes place continuously during both the heating and cooling semiperiods, can be deduced [28]. The event is more marked and appreciable after the more prolonged crystallization time, which suggests that the intensity of the irreversible process increases with the annealing time. As previously proven [21], the irreversible thermal event revealed by the annealing peak is due to the enthalpy recovery that accompanies the mobilization of the rigid amorphous fraction and that occurs simultaneously with the initial melting of the crystals isothermally developed [21]. Thus the annealing peak has to be ascribed to initial melting of crystals with overlapping of an enthalpic event associated to RAF mobilization.

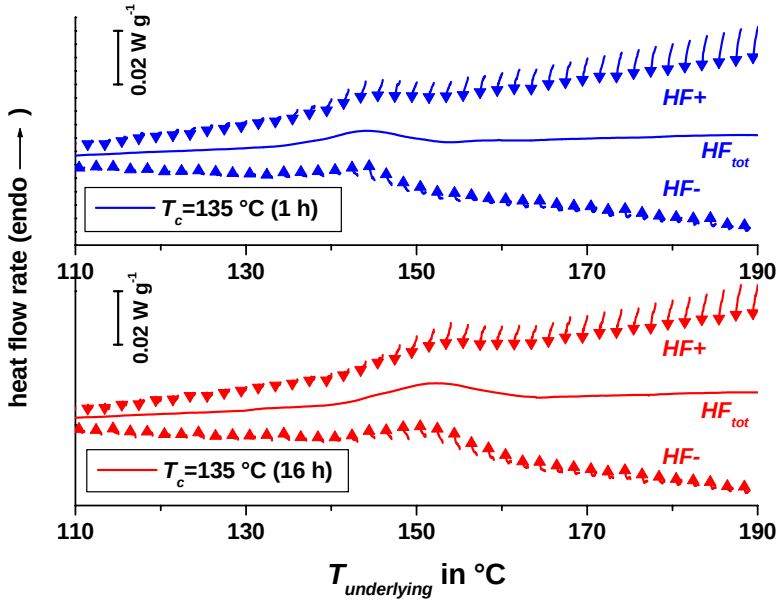

Fig. 7. Steady-state heat flow rate curves of PET in the heating and cooling semiperiods (*HF+* and *HF-* respectively), after isothermal crystallization for 1 h and 16 h at 135 °C (blue and red lines respectively), as a function of the underlying temperature in a restricted temperature range (see Figure 6). The initial points of the steady-state are evidenced by symbols (heating semiperiod: ▼; cooling semiperiod: ▲). The total heat flow rate curve (HF_{tot}) is also drawn. The *HF+* and *HF-* curves have been shifted closer to HF_{tot} by fixed amounts.

As demonstrated, the use of the initial steady-state points allows to recognize and separate the irreversible thermal events occurring during the TMDSC scan; in particular, initial steady-state points dissimilar from the baseline heat flow rate prove the occurrence of endothermic or exothermic irreversible processes [21]. From Figure 6 it can be evidenced that both melting and crystallization/recrystallization are irreversible, i.e. they occur continuously during cooling and heating semiperiods, to different extent and in different temperature ranges: melting is highly irreversible from about 250 °C to the end of the process while crystallization/recrystallization is irreversible from 145 °C to 250 °C.

Since the initial steady-state heat flow rate points of the heating and cooling semiperiods contain information on the irreversible events that continue from the previous cooling or heating semiperiods respectively [21], whereas the total heat flow rate results from the algebraic sum of all the endothermic and exothermic events occurring during both the semiperiods, a comparison between the $c_{p,tot}$ and the specific heat capacities from the initial steady-state points can yield to an estimation of the relative percentages of fusion-crystallization/recrystallization and enthalpy recovery that occur in correspondence with the annealing peak.

Figure 8 shows $c_{p,tot}$ and the specific heat capacities c_{p+} and c_{p-} calculated from the heat flow rate initial steady-state points for the PET samples crystallized for 1 h and 16 h respectively, in the temperature range 120-180 °C. The c_{p+} curves exhibit an increase starting from 135 °C and 140 °C respectively, up to approximately 145 °C and 152 °C, then the values decrease due to irreversible crystallization. Also c_{p-} deviates from the baseline linear trend at 135 °C and 140 °C respectively, but in this

case the values reduce since the irreversible thermal event is endothermic. At temperatures higher than 145 °C and 152 °C the c_{p-} values increase markedly because of the irreversible crystallization process. It is worth noting that the peaks described by $c_{p,tot}$ curves appear higher than those relative to c_{p+} and c_{p-}, which confirms that, besides enthalpy recovery, also fusion contribute to the small endotherm above T_c.

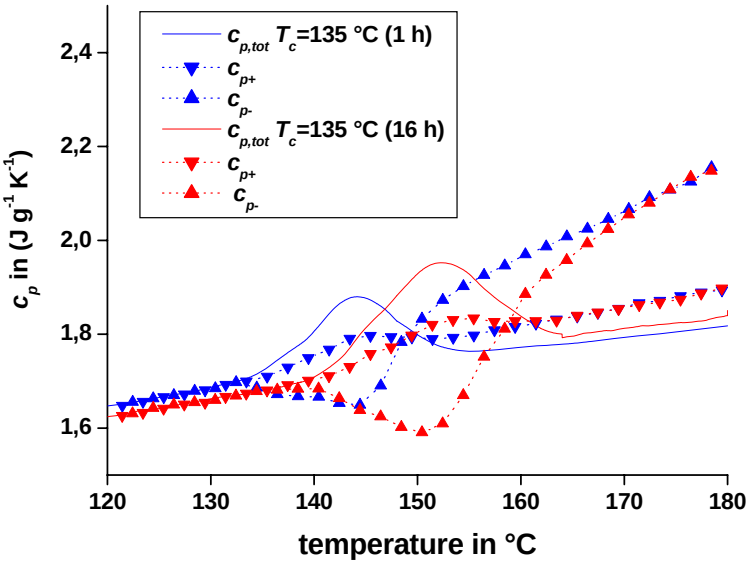

Fig. 8. Total specific heat capacity ($c_{p,tot}$) and specific heat capacities calculated from the initial steady-state points in the heating and cooling semiperiods (c_{p+} and c_{p-} respectively) for PET, after isothermal crystallization for 1 h and 16 h at 135 °C (blue and red symbols respectively), as a function of the underlying temperature, in the temperature range 120-180 °C.

Due to the overlapping of irreversible crystallization, calculation of the areas under the $c_{p,tot}$, c_{p+} and c_{p-} curves was performed from 135 °C and 140 °C respectively only up to the peak of $c_{p,tot}$ plots, using as baseline the extrapolation of the specific heat capacity below the annealing peak. As a consequence the calculated values refer only to about one half of the thermal events under investigation. The enthalpy values obtained from the $c_{p,tot}$, c_{p+} and c_{p-} curves are 0.60 J g^{-1}, 0.22 J g^{-1} and 0.34 J g^{-1} respectively for the PET sample crystallized for 1 h at 135 °C and 1.4 J g^{-1}, 0.40 J g^{-1} and 1.00 J g^{-1} respectively for the PET sample crystallized for 16 h at 135 °C (Obviously the sign of the area under c_{p-} has been changed because it refers to cooling steps). It is worth noting that the enthalpy calculated from the c_{p-} data is higher with respect to that from the c_{p+} curve, since the c_{p-} data refer to the intensity of the irreversible process in the previous heating semiperiods, in which the enthalpy recovery is expected higher [30].

The average values between the areas under c_{p+} and the areas under c_{p-} can be used to estimate the enthalpy that is retrieved during the TMDSC scan due to mobilization of the RAF (0.28 J g^{-1} for PET crystallized for 1 h at 135 °C and 0.70 J g^{-1} for PET crystallized for 16 h at 135 °C). Since the enthalpy calculated from $c_{p,tot}$ accounts for both the irreversible enthalpy recovery and the average enthalpy for fusion and crystallization/recrystallization, it comes out that for PET crystallized at

135 °C for 1 and 16 h, approximately half of the area measured in correspondence with the small endotherm arises from the irreversible enthalpy recovery that follows the structural relaxation of the RAF. Such estimation is independent of the length of the annealing time and demonstrates that during the isotherm at 135 °C the increase of crystallinity and the densification of the rigid amorphous fraction go parallel by chance. Unluckily, the RAF amount that mobilizes in correspondence of the annealing peak cannot be precisely quantified. In fact it is likely that not all the rigid amorphous fraction devitrifies in the range 130-160 °C, since the RAF in PET should be completely mobilized at temperatures higher than 180 °C [16, 31].

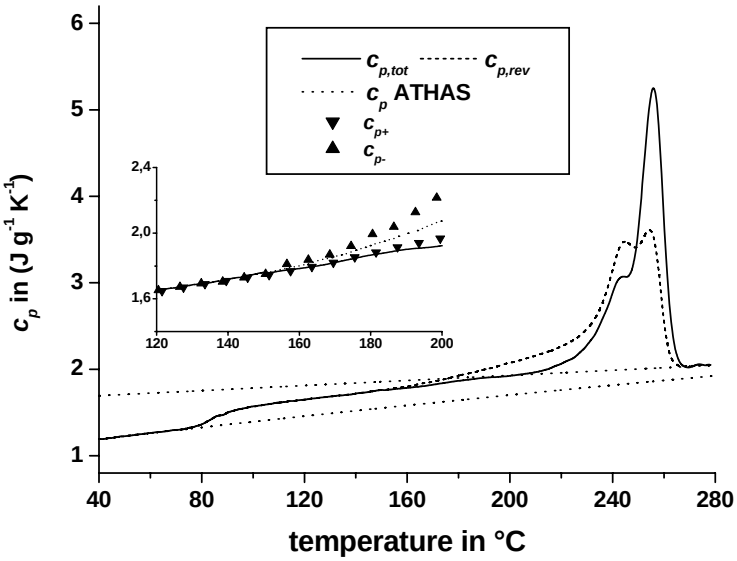

Fig. 9. Total specific heat capacity ($c_{p,tot}$: solid line) and reversing specific heat capacity ($c_{p,rev}$: dash line) of PET as a function of the underlying temperature, after non isothermal crystallization at -2 °C min^{-1}. The crystalline and mobile amorphous specific heat capacities, as taken from ATHAS Data Bank [22], are also shown as dot lines. In the inset the total specific heat capacity, the reversing specific heat capacity and the specific heat capacities calculated from the initial steady-state points in the heating and cooling semiperiods (c_{p+} and c_{p-} respectively) are reported in a restricted temperature range.

Figure 9 illustrates the total and reversing specific heat capacity curves of PET from TMDSC, after non-isothermal crystallization at -2 °C min^{-1}. No annealing peak appears in the $c_{p,tot}$ curve, whereas both $c_{p,tot}$ and $c_{p,rev}$ display a small step from about 160 °C. This increase can be connected both with the beginning of the melting process, since crystallization was found to extend on cooling down to 140 °C (Figure 1) and the mobilization of the RAF that occurs progressively and simultaneously with the melting of the poorest and/or most defective crystals with which it is coupled. The devitrification of the rigid amorphous fraction takes place without enthalpy recovery, as also evidenced in the inset of Figure 9, that shows how the c_{p+} and c_{p-} curves do not describe any peak in the temperature interval in which $c_{p,tot}$ and $c_{p,rev}$ display a step. At temperatures lower than 160 °C, the mobilization of the RAF could take place around the same temperature at which it develops, starting form the bulk glass transition and with a trend similar to that reported in Figure 3. Also this experiment

proves that the structural relaxation of the RAF occurs during the isotherm at the crystallization temperature.

Conclusions

Our analysis on the kinetics of solidification of PET reveals that, during crystallization from the melt, the rigid amorphous fraction starts to vitrify when the crystallization process is almost completed and develops further on cooling down to the glass transition of the bulk amorphous phase. As seen in Figure 3, most of the RAF vitrifies in the temperature range between 175 and 100 °C, in correspondence of only a minor increment of the crystal fraction.

The smooth tail in the low temperature side of the crystallization exotherm seen in Figure 1, together with the the slight increment of the m_C curve at temperatures lower than 180 °C,, quantified in Figure 3, point to the occurrence of secondary crystallization in this temperature range. This is confirmed by literature data, that prove growth of large amounts of secondary crystals in poly(ethylene terephthalate) after primary crystallization [32]. The exact nature of secondary crystallization in semicrystalline polymers is still under debate. It has been hypothesized that it can include thickening of lamellae, perfection of the crystals, as well growth of defective crystallites [32]. It was also suggested that the mechanism can be influenced by restrained amorphous regions, where entropy is reduced due to the presence of neighboring crystalline stacks [33-34]. Our results of simultaneous development of rigid amorphous fraction and secondary crystals confirm this hypothesis. The growing secondary lamellae cause geometrical restrictions in the rearrangements of the amorphous regions localized in their proximity, which results in formation of the RAF.

Similarly, our analysis of the small endotherm located a few degrees above T_c shows a relation between partial mobilization of the RAF and fusion of the smaller and/or more defective crystals. It is likely that melting of secondary crystal is controlled not only by constraints exerted by the neighboring crystallites, but also by possible induced rigidity in the amorphous chain portions. Upon heating, enhancement of chain mobility in the amorphous area favors fusion of thinner lamellae, which in turn, reduces geometrical restrictions and allows release of strain in the interfacial area between the crystals and the surrounding amorphous regions. After isothermal crystallization, this coupled process is revealed by enthalpy recovery and mobilization of strained amorphous segments, which occur simultaneously with the initial melting of the semicrystalline polymer.

Summarizing, some mutual influence between RAF vitrification and insertion of secondary lamellae, as well as between RAF mobilization and partial melting seems to be active. Restrictions of chain mobility in the crystallizing environment parallel the end of primary crystal growth, as well as the occurrence of initial devitrification of the RAF permits the onset of melting of the thinner and/or more defective crystals.

Experimental part

Poly(ethylene terephthalate) (PET) of molar mass M_w = 21,400g mol^{-1} was kindly received through the Bank of Crystallizable Polymers of European funded COST Action P12 [35]. After drying under vacuum at 100 °C for 16 h, the sample chips were compression-molded with a Carver Laboratory Press at a temperature of 280 °C for 3 min, without any applied pressure, to allow complete melting. After this period, a load

of about 0.5 ton was applied for 2 min. Successively the sample was quickly cooled to room temperature by means of cold water circulating in the plates of the press.

DSC and TMDSC measurements were performed with a Perkin-Elmer Differential Scanning Calorimeter DSC7. The instrument was calibrated in temperature with high purity standards (indium, naphthalene and cyclohexane) according to the procedure for standard DSC. The heat-flow rate was initially calibrated with the heat of fusion of indium, then refined with a run of two empty aluminum pans, and a calibration run with sapphire as a standard for both DSC and TMDSC experiments [36]. Dry nitrogen was used as purge gas at a rate of 30 ml min^{-1}. The sample mass was kept small, approximately equal to 4 mg, to reduce as much as possible the problems that may arise from thermal gradients inside the sample, especially during non-isothermal crystallization [37]. A fresh sample was employed for each analysis in order to minimize thermal degradation.

Non-isothermal crystallization was conducted by conventional DSC and TMDSC on compression-molded PET samples previously heated from room temperature to 280 °C at a rate of 30 °C min^{-1} and maintained at this temperature for 3 min. For the conventional DSC analyses the samples were cooled to 40 °C at the scanning rate of -2 °C min^{-1}. After the non-isothermal crystallization at -2 °C min^{-1}, a TMDSC analysis was carried out on heating at the underlying scanning rate of 2 °C min^{-1}, with a temperature amplitude (A_T) of 1.0 °C and a period (p) of 60 s (heating semiperiod rate: 6 °C min^{-1}, cooling semiperiod rate: -2 °C min^{-1}). The TMDSC measurements were designed using the dynamic temperature program that is obtained through a sawtooth modulation in the Perkin-Elmer DSC. Non-isothermal crystallization was also performed by TMDSC with A_T = 1.0°C, p = 60 s at the underlying scanning rate of -2 °C min^{-1}.

Isothermal crystallizations were conducted after melting the polymer at 280 °C for 3 min and cooling to the desired crystallization temperature (T_c) at a nominal rate of 200 °C min^{-1}. The lengths of the isothermal step were 1 h and 16 h. After isothermal crystallization, the samples were quenched to 30 °C, then DSC and TMDSC analyses were performed upon heating. Conventional DSC measurements after isothermal crystallization were conducted at a heating rate of 10 °C min^{-1}, whereas the TMDSC measurements were performed with A_T = 1.0°C and p = 60 s at an underlying scanning rate of 2 °C min^{-1}.

From TMDSC measurements the total specific heat capacity ($c_{p,tot}$), approximately equal to the total specific heat capacity from conventional DSC, and the reversing specific heat capacity ($c_{p,rev}$) can be obtained. The total specific heat capacity ($c_{p,tot}$), is derived from the total heat flow rate (HF_{tot}), obtained by averaging the measured heat flow rate over the modulation period [38-39], whereas the reversing specific heat capacity ($c_{p,rev}$) is obtained from the ratio of the amplitudes of modulated heat flow rate ($A_{\Phi,n}$) and temperature ($A_{T,n}$), both approximated with Fourier series [38-39]:

$$c_{p,rev}(\omega,n,t) = \frac{A_{\Phi,n}(t)}{A_{T,n}(t)} \frac{K(\omega,n,t)}{mn\omega} \tag{9}$$

where t is the time, n the order of the harmonic, ω the base modulation frequency (ω=2π/p), m the mass of the sample and $K(n,\omega,t)$ the frequency-dependent calibration factor. The reversing specific heat capacity values reported in this contribution were obtained from the first harmonics of the Fourier series. From the calibration of the heat flow rate with sapphire, the K factor was 1.05 for p = 60 s. The

correctness of the calibration factor was proven by the good agreement of the measurements with the ATHAS data bank information included in the results.

The experimental curves shown are the average of four repeated runs.

References

[1] Suzuki, H.; Grebowicz, J.; Wunderlich, B. *Br. Polym. J.* **1985**, *17*, 1.
[2] Cheng, S.Z.D.; Cao, M.Y.; Wundelich B. *Macromolecules* **1986**, *19*, 1868.
[3] Wunderlich, B. *Progr. Polym. Sci.* **2003**, *28*, 383.
[4] Kitamaru, R.; Horii, F.; Murayama, K. *Macromolecules* **1986**, *19*, 636.
[5] Kunz, M.; Möller, M.; Heinrich, U.R.; Cantow, H.J. *Makromol. Chem. Macromol. Symp.* **1988**, *20/21*, 147. **1989**, *23*, 57.
[6] Gabriels, W.; Gaur, H.A.; Feyen, F.C.; Weeman, W.S. *Macromolecules* **1994**, *27*, 5811.
[7] Cheng, J.; Fone, M.; Reddy, V.N.; Schwartz, K.B.; Fisher, H.P.; Wunderlich, B. *J. Polym. Sci.: Part B: Polym. Phys.* **1994**, *32*, 2683.
[8] Litvinov, V.M.; Mathot, V.B.F. *Solid State Magn. Reson.* **2002**, *22*, 218.
[9] Pak, J.; Pyda, M.; Wunderlich, B. *Macromolecules* **2003**, *36*, 495.
[10] Righetti, M.C.; Di Lorenzo, M.L.; Angiuli, M.; Tombari, E. *Macromolecules* **2004**, *37*, 9027.
[11] Alsleben, M.; Schick, C. *Thermochim. Acta* **1994**, *238*, 203.
[12] Schick, C.; Wurm, A.; Mohammed, A. *Coll. Polym. Sci.* **2001**, *279*, 800.
[13] Schick, C.; Wurm, A.; Mohammed, A. *Thermochim. Acta* **2003**, *396*, 119.
[14] Xu, H.; Ince, S.; Cebe, P. *J. Polym. Sci.: Part B: Polym. Phys.* **2003**, *41*, 3026.
[15] Androsch, R.; Wunderlich, B. *Polymer* **2005**, *46*, 12556.
[16] Righetti, M.C.; Tombari, E.; Angiuli, M.; Di Lorenzo, M.L. *Thermochim. Acta* **2007**, *462*, 15.
[17] Righetti, M.C; Tombari, E.; Di Lorenzo, M.L.; *Eur. Polym. J*. in press, doi:10.1016/j.eurpolymj.2008.05.026.
[18] Song, M. *J. Appl. Polym. Sci.* **2001**, *81*, 2779.
[19] Lu, S.X.; Cebe, P. *Polymer* **1996**, *37*, 4857.
[20] Xu, H.; Ince, S.; Cebe, P. *J. Polym. Sci.: Part B: Polym. Phys.* **2003**, *41*, 3026.
[21] Righetti, M.C.; Di Lorenzo, M.L.; Tombari, E. Angiuli, M. *J.Phys.Chem B.* **2008**, *112*, 4233.
[22] ATHAS Data Bank, M. Pyda M. (Ed.), Web address: http://www.prz.rzeszow.pl/athas/databank/intro.html.
[23] Goderis, B.; Reynaers, H.; Scherrenberg, R.; Mathot, V.B.F.; Kock, M.H.J. *Macromolecules* **2001**,*34*,1779.
[24] Merzlyakov, M.; Schick, C. *J. Thermal Anal. Calorim.* **2000**, *61*, 649.
[25] Mathot, V.B.F.; Scherrenberg, R.L.; Pijpers, M.F.J.; Bras, W. *J. Thermal Anal.* **1996**, *46*, 681.
[26] Mathot, V.B.F. in: Mathot, V.B.F. (Ed.) *Calorimetry and Thermal Analysis of Polymers*, Hanser/Gardner, Cincinnati, **1994**; p 105.
[27] Righetti, M.C; Di Lorenzo, M.L. *in preparation*
[28] Di Lorenzo, M.L.; Wunderlich, B. *Thermochim. Acta* **2003,** *405*, 255.
[29] Hutchinson, J. **1998,** *324*, 165.
[30] Weyer, S.; Merzlyakov, M.; Schick, C. *Thermochim. Acta* **2001**, *377*, 85.
[31] Okazaki, I.; Wunderlich, B. *Macromolecules* **1997**, *30*, 1758.
[32] Wang, Z.-G.; Hsiao, B.S.; Sauer, B.B.; Kampert, W.G. *Polymer* **1999**, *40*, 4615.

[33] Hsiao, B.S.; Sauer, B.B.; Verma, R.; Chu, B.; Harney, P.; Zachmann, H.G.; Seifert, S. *Macromolecules* **1995**, *28*,6931.
[34] Sohn, S.; Alizadeh, A.; Marand, H. *Polymer* **2000**, *41*, 8879.
[35] COST P12 ACTION web site: http://www.uni-rostock.de/fakult/ manafak/physik/ poly/COST_P12/index.htm.
[36] Archer, D.G.; *J. Phys. Chem. Ref. Data* **1993**, *22*, 1441.
[37] Di Lorenzo, M.L.; Cimmino, S.; Silvestre, C. *Macromolecules* **2000**, *33*, 3828.
[38] Wurm, A.; Merzlyakov, M.; Schick, C. *Coll. Polym. Sci.* **1998**, *276*, 289.
[39] Androsch, R.; Moon, I.; Kreitmeier, S.; Wunderlich, B. *Thermochim. Acta* **2000**, *357-358*, 267.